

# An Eulerian method for computing multi-valued solutions of the Euler-Poisson equations and applications to wave breaking in klystrons

Xiantao Li,<sup>1</sup> John G. Wöhlbier,<sup>2</sup> Shi Jin,<sup>3</sup> and John H. Booske<sup>2</sup>

<sup>1</sup>*The Program in Applied and Computational Mathematics,  
Princeton University, Princeton, New Jersey 08544*

<sup>2</sup>*Department of Electrical and Computer Engineering, University of Wisconsin – Madison 53706*

<sup>3</sup>*Department of Mathematics, University of Wisconsin – Madison 53706*

(Dated: November 13, 2003)

We provide new methods of computing multi-valued solutions to the Euler-Poisson system and test them in the context of a klystron amplifier. An Eulerian formulation capable of computing multi-valued solutions is derived from a kinetic description of the Euler-Poisson system and a moment closure. The system of the moment equations may be closed due to the special structure of the solution in phase space. The Eulerian moment equations are computed for a velocity modulated electron beam, which has been shown by prior Lagrangian theories to break in a finite time and form multi-valued solutions. The results of the Eulerian moment equations are compared to direct computation of the kinetic equations, a Lagrangian method also developed in the paper, and a prior analytical theory for two cases. We use the Lagrangian formulation for the explicit computation of wave breaking time and location for typical velocity modulation boundary conditions.

PACS numbers: 52.35.Mw, 52.35.Tc, 52.65.Ff, 84.40.Fe

## I. INTRODUCTION

The phenomenon of wave breaking in systems described by fluid equations is widely documented [1]. Different physical systems and their associated model equations may require that their wave breaking events be handled in different manners. Where the physics of one system may dictate that a shock develops after the wave breaking event, the physics of another system may dictate that the formation of multi-valued solutions is appropriate after the wave breaking event. Physical systems where multi-valued solutions may be appropriate include geometric optics, arrival time in seismic imaging, semi-classical limits of the linear and nonlinear Schrödinger equations, integrable systems (such as the nonlinear Korteweg-de Vries equation) in the small dispersion regimes, nonlinear plasma waves, stellar dynamics and galaxy formation, multi-lane traffic flows, and electron overtaking in the electron beams of vacuum electronics devices. Direct Eulerian formulations of such systems based on the classical WKB analysis, which usually introduces viscosity solutions, may fail when the physical solution is the one which becomes multi-valued after wave breaking.

Recently, there has been a growing interest in developing an Eulerian framework for the computation of the multi-valued solutions that arise in geometric optics [2–6] and in the semi-classical limit of the Schrödinger equation [7–10]. An Eulerian method may be preferred over a Lagrangian method since the former computes the numerical solution of partial differential equations on a fixed grid, while the latter may lose accuracy or need regridding as the rays expand.

In this paper we consider a system of Euler-Poisson equations. The Euler-Poisson equations have applications to many physical problems including fluid dynam-

ics, plasma dynamics, gas dynamics, elasticity, gaseous stars, quantum gravity, general relativity, rigid bodies, and semiconductors. While it is known that for certain initial conditions the solution of the Euler-Poisson system can break [11], methods for computing its multi-valued solutions using Eulerian methods have not been reported.

The main result of this paper is an Eulerian method for solving the Euler-Poisson system that can capture multi-valued solutions beyond wave breaking. The method is based on a kinetic formulation and an exact moment closure. For comparison, we also give a Lagrangian formulation which is solved analytically prior to wave breaking, and numerically to include the multi-valued solutions. An application of the method to a modulated electron beam as found in a klystron amplifier is given and results of the methods are compared to an analytic theory of the klystron by Lau *et al.* [12].

In Section II we describe the principle of operation for a klystron amplifier, and we present an Euler-Poisson model of the system. The Eulerian methods are developed in Section III. A kinetic formulation for the Euler-Poisson system is given first, using the Vlasov-Poisson system, which is then closed using an *exact* moment closure to derive multi-phase equations in the physical space. This is the main result of the paper. In Section IV we present a Lagrangian formulation of the system. Numerical examples comparing the methods are given in Section V. Section VI discusses the computation of breaking time and location. The paper is concluded in Section VII. There are several supplemental appendices providing details of numerical methods and analytical computations.

## II. AN EULER-POISSON MODEL OF A MODULATED ELECTRON BEAM

A wide variety of vacuum electronics devices constitute a large fraction of today's high power, high frequency electromagnetic wave sources and amplifiers [13]. The source of energy for amplification in a vacuum electronics device is a high energy beam of electrons that interacts with an electromagnetic wave. The class of vacuum electronics devices known as "linear beam devices" use electron beam velocity modulation to obtain amplified electron beam current modulation, which is converted into amplified electromagnetic radiation.

The simplest example of a linear beam device is a two-cavity klystron [14]. The geometry of the two cavity klystron is shown in Fig. 1. The basic components of

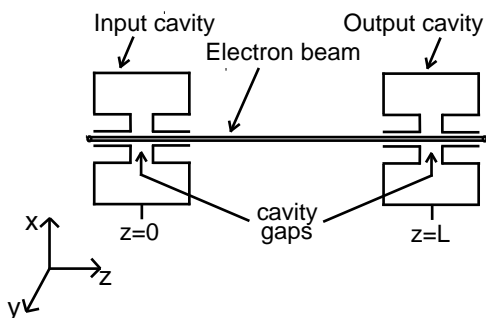


FIG. 1: Two cavity klystron geometry. The signal on the input cavity imparts a velocity modulation on the electron beam, which is streaming from left to right in the figure. The velocity modulation is converted to a beam current modulation downstream, which induces an amplified version of the input signal in the output cavity.

the device are an input cavity, an output cavity, and an electron beam. The cavities are resonant electromagnetic cavities whose resonant frequencies are equal to the operational frequency of the amplifier. The electron beam is passed through the input cavity where it experiences the electric field of the cavity "gap," and subsequently passes through the output cavity where it induces electromagnetic fields in the output cavity. The radio frequency (RF) signal injected into the input cavity results in a time-varying electric field in the input cavity gap. As the electron beam passes through the gap the time-varying gap electric field imparts a "modulation" on the electrons in the beam. In particular, an electron is accelerated or decelerated depending on the phase of the gap electric field during the instant at which the electron passes through the gap. As the "velocity modulation" is carried by the dc beam velocity to the output cavity the velocity modulation transforms to a beam density and beam current modulation. Finally, as the current modulation passes through the output cavity it induces an RF signal which is an amplified version of the input RF signal. However, due to the nonlinear evolution of the electron beam, the spectra of the beam current modu-

lation and the RF output signal are distorted from the spectrum of the original RF input signal.

For strong enough input RF "drive," some electrons are sped up sufficiently such that they pass by, or "overtake," other electrons that were initially ahead of them before they reach the output cavity. In a 1-dimensional Eulerian description of the electron beam, a multi-valued velocity function is required to describe the electron beam behavior when the beam has experienced "overtaking."

To simplify our analysis we model a 1-d velocity modulated electron beam and for the time being ignore coupling of the beam current to an output cavity. Required for the model are a charge conservation equation, a momentum balance equation (Newton's law) where the force on electrons is due to the internal "Coulomb repulsion," or "space charge" electric field, and Gauss' law to determine the evolution of the space charge electric field. The governing equations are the following Euler-Poisson system [12]

$$\begin{cases} \frac{\partial}{\partial t}\rho + \frac{\partial}{\partial z}(\rho u) = 0 \\ \frac{\partial}{\partial t}(\rho u) + \frac{\partial}{\partial z}(\rho u^2) = \frac{e}{m_e} R_{sc} E \rho \\ \frac{\partial E}{\partial z} = \frac{\rho - \rho_0}{\epsilon_0} \end{cases} \quad (1)$$

subject to the boundary conditions

$$\begin{cases} \rho(0, t) = \rho_0, \\ u(0, t) = u_0 + u_0 \frac{\epsilon(t)}{2}, \\ E(0, t) = 0, \end{cases}$$

where  $\rho(z, t)$  is the electron beam charge density,  $u(z, t)$  is the electron beam velocity, and  $E(z, t)$  is the space charge electric field. The function  $\epsilon(t)$  represents an arbitrary time dependent modulation of the electron beam velocity at location  $z = 0$ . The "space charge reduction factor"  $R_{sc}$  accounts for the finite radius of the electron beam by reducing the accelerating electric field an electron experiences [14][22]. The variables  $e$ ,  $m_e$ , and  $\epsilon_0$  represent electron charge, electron mass, and permittivity of free space, respectively. The dc beam charge density  $\rho_0$  and dc beam velocity  $u_0$  are determined by the dc beam current, dc beam voltage, and beam radius (see Section V).

In order to make our formulation more generic, and the numerical procedures more convenient and effective, we choose the following characteristic quantities

$$Z = L, \quad U = u_0, \quad T = \frac{Z}{U}, \quad D = \rho_0,$$

where  $L$  is the klystron length (see Section V), and define the non-dimensional variables

$$z^* = \frac{z}{Z}, \quad u^* = \frac{u}{U}, \quad t^* = \frac{t}{T}, \quad \rho^* = \frac{\rho}{D}, \quad E^* = \frac{\epsilon_0 E}{ZD}.$$

One arrives at the re-scaled equations

$$\begin{cases} \frac{\partial}{\partial t^*}\rho^* + \frac{\partial}{\partial z^*}(\rho^* u^*) = 0, \\ \frac{\partial}{\partial t^*}(\rho^* u^*) + \frac{\partial}{\partial z^*}(\rho^* u^{*2}) = \hat{R}_{sc} \rho^* E^*, \\ \frac{\partial E^*}{\partial z^*} = \rho^* - 1. \end{cases} \quad (2)$$

with

$$\hat{R}_{sc} = \frac{eZDT}{m_e \epsilon_0 U} R_{sc} = \omega_p^2 T^2 R_{sc} \quad (3)$$

and the boundary conditions

$$\rho(z=0, t) = \rho^0(t) = 1, \quad u(z=0, t) = u^0(t) = 1 + \frac{\epsilon(t)}{2}$$

where the normalized star (\*) notation has been dropped. A case of general interest in klystrons is

$$u^0(t) = 1 + \frac{1}{2} \sum_n \epsilon_n \sin(\omega_n T t + \theta_n). \quad (4)$$

In this case, we will normalize the frequency  $\omega_n$  to  $\omega_n T$  so that the scaling factor  $T$  will not appear in derivations. The term  $\omega_p$  introduced in Eq. (3) is the plasma frequency [14]. Finally, we would point out that our analysis and numerical methods are not restricted to a constant input density  $\rho^0(t) = 1$ . We will use the notation  $\rho^0(t)$  or  $\rho^0$  to represent a generic density boundary condition, even though all the numerical results are carried out for  $\rho^0 = 1$ .

### III. EULERIAN METHODS

#### A. A kinetic approach

It is known that the solution of the Euler-Poisson system can break in finite time [11], and that the density  $\rho(z, t)$  will display the concentration effect (usually called a  $\delta$ -shock), whereas the velocity will develop a shock profile. After the solution breaks, there are different ways to interpret the solution. Conventionally the solution is obtained in the limit of zero viscosity. Numerical evidence shows that this allows shock propagation. However, in some circumstances, such as a modulated electron beam, one expects the ‘‘overtaking’’ phenomena, i.e., the solution of the Euler-Poisson system becomes multi-valued.

To interpret the multi-valued solutions of the Euler-Poisson equations, we propose the following so-called Vlasov-Poisson equations for the kinetic distribution  $w(z, v, t)$ ,

$$\begin{cases} w_t + v w_z + \hat{R}_{sc} E(z, t) w_v = 0, \\ \frac{\partial}{\partial z} E = \int_{\mathbb{R}^+} w(z, v, t) dv - 1, \\ (z, v, t) \in \mathbb{R} \times \mathbb{R}^+ \times \mathbb{R}^+, \end{cases} \quad (5)$$

with the boundary value,

$$w(0, v, t) = \rho^0(t) \delta(v - u^0(t)). \quad (6)$$

In order to make the connection to the Euler-Poisson equations we define,

$$\rho = \int_{\mathbb{R}^+} w(z, v, t) dv, \quad I = \int_{\mathbb{R}^+} w(z, v, t) v dv$$

as charge density and current density functions. If one assumes that the solution to Eqs. (5) remains as a delta function (as will be justified for the single phase case), i.e.,

$$w(z, v, t) = \rho(z, t) \delta(v - u(z, t)),$$

one can multiply the Vlasov-Poisson equations by 1 and  $v$ , integrate with respect to  $v$  and obtain the Euler-Poisson equations (2). This indicates the equivalence of the Vlasov-Poisson equations and the Euler-Poisson system when the solution is single-valued. As the solution becomes multi-valued, the introduction of the phase variable  $v$  naturally incorporates all of the possible values in the solution.

To solve Eqs. (5), we define its ‘‘bicharacteristic curves’’  $(s, t(v_0, t_0; s), v(v_0, t_0; s))$ ,

$$\begin{cases} \frac{d}{ds} t = 1/v, & t = t_0 \text{ at } s = 0, \\ \frac{d}{ds} v = \hat{R}_{sc} E/v, & v = v_0 \text{ at } s = 0, \\ z = s. \end{cases} \quad (7)$$

Equations (7) define a mapping

$$(v_0, t_0) \in \mathbb{R}^+ \times \mathbb{R}^+ \rightarrow (v, t) \in \mathbb{R}^+ \times \mathbb{R}^+.$$

We assume that this mapping is smooth. This is not a mathematically rigorous result. It has not been proven true mathematically for general initial or boundary value problems of the Vlasov-Poisson system (5). However, for the numerical examples given in this paper, this assumption seems valid based on the numerical evidence given in Section V.

To check the invertibility of the mapping we consider the associated Jacobian,

$$\Delta = \det \left( \frac{\partial(v, t)}{\partial(v_0, t_0)} \right).$$

By direct differentiation one can verify that

$$\frac{d}{ds} (v \Delta) = 0. \quad (8)$$

In light of the initial conditions we get from Eq. (8)

$$\Delta(v_0, t_0; s) = v_0 / v(v_0, t_0; s). \quad (9)$$

Since we only consider cases when  $v(v_0, t_0; s) > 0$ , Eq. (9) implies that the mapping  $(v_0, t_0) \rightarrow (v, t)$  is invertible. We use  $(t_0(v, t; s), v_0(v, t; s))$  to represent the inverse transform.

Simple computation using (5) shows that

$$\frac{d}{ds} w(s, v(v_0, t_0; s), t(v_0, t_0; s)) = 0.$$

Therefore along the bicharacteristic curves the solution of (5) remains invariant,

$$\begin{aligned} w(z, v, t) &= w(0, v_0(v, t; z), t_0(v, t; z)), \\ &= \rho^0(t_0(v, t; z)) \delta(\Phi_{zt}(v)), \end{aligned}$$

with

$$\Phi_{zt}(v) = v_0(v, t; z) - u^0(t_0(v, t; z)). \quad (10)$$

If the kernel of  $\Phi_{zt}(v)$   $\{v : \Phi_{zt}(v) = 0\}$  has finitely many elements  $\{u_k, k = 1, 2, \dots, N(z, t)\}$ , then  $\delta(\Phi_{zt}(v))$  can be split up and the solution of Eqs. (5) can be written as

$$w(z, v, t) = \sum_{k=1}^N \rho_k \delta(v - u_k), \quad \rho_k = \rho^0 |\Phi'_{zt}(u_k)|^{-1}. \quad (11)$$

This form of the solution will be used to close the moment system of the Euler-Poisson equations (5), just as the local Maxwellian closes the moment system of the Boltzmann equation. This linear superposition was obtained first for the linear Vlasov equation where the potential is independent of the solution (external potential) in Refs. [8, 15].

One can verify that each pair  $(\rho_k, u_k)$  given above satisfies the Euler-Poisson system. This was proved for the linear Vlasov equation in Ref. [8] and the same argument holds here. Therefore, the kinetic formulation provides a way to recover the multi-valued solutions to the Euler-Poisson system.

Meanwhile, as the solution becomes multi-valued, we have,

$$\rho = \int w(x, v, t) dv = \sum_{k=1}^N \rho_k,$$

$$I = \int w(x, v, t) v dv = \sum_{k=1}^N \rho_k u_k.$$

Namely, the charge density and current density comply with the linear superposition principle even though each individual phase is governed by a nonlinear system.

Figure 2 provides an illustration of the evolution in  $z$  of a constant  $w(z, v, t)$  curve for which the solution in the physical space becomes three phased.

## B. Multi-phase equations in the physical space

The kinetic equation can certainly be solved via standard finite difference discretization using the upwind scheme or a particle method. However, computations based on the discretization of phase space or a collection of interacting particles can be very expensive, especially when one attempts to achieve good resolution. We thus aim at establishing a system defined only in the *physical space* to describe the multi-phase phenomena. This technique is motivated by the kinetic theory of gas dynamics and is usually called kinetic moment closure [16–18]. Unlike the usual moment closure for a general kinetic (Boltzmann) equation, which uses an *ad hoc* form of density distribution and therefore obtains an approximate moment system, here we have obtained the *exact* moment closure using Eq. (11).

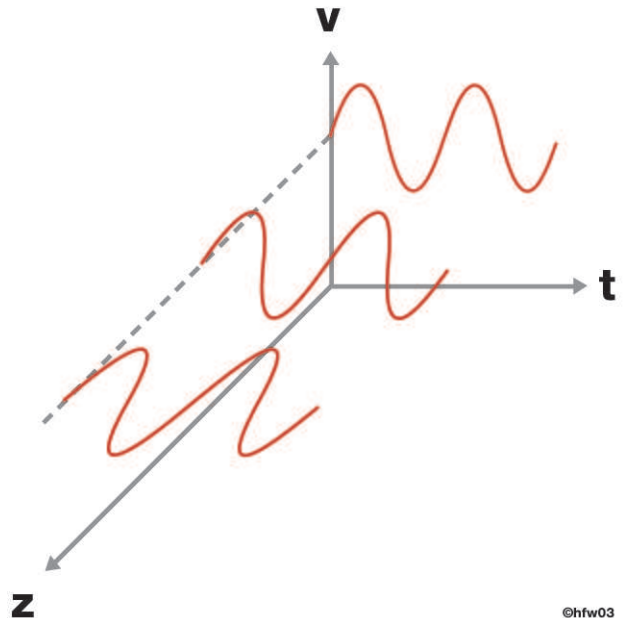


FIG. 2: Illustration of evolution in  $z$  of a constant  $w(z, v, t)$  curve for which the solution in the physical space becomes three phased.

We first define the moments of the Vlasov-Poisson equation,

$$m_l = \int_{\mathbb{R}^+} w(z, v, t) v^l dv, \quad l = 0, 1, \dots, 2N. \quad (12)$$

Then taking moments of Eqs. (5) one gets,

$$\begin{aligned} \frac{\partial}{\partial t} m_0 + \frac{\partial}{\partial z} m_1 &= 0, \\ \frac{\partial}{\partial t} m_1 + \frac{\partial}{\partial z} m_2 &= \hat{R}_{sc} m_0 E, \\ \dots + \dots &= \dots, \\ \frac{\partial}{\partial t} m_{2N-1} + \frac{\partial}{\partial z} m_{2N} &= (2N-1) \hat{R}_{sc} m_{2N-2} E, \quad (13) \\ \frac{\partial E}{\partial z} &= \sum_{k=1}^N \rho_k - 1. \end{aligned}$$

In order to close this system, and to be able to advance the system in the  $z$  direction, we need to represent  $m_0$  in terms of  $(m_1, m_2, \dots, m_{2N})$ . From Eq. (11) one can express the moments in terms of  $(\rho_k, u_k)$ 's:

$$m_l = \sum_{k=1}^N \rho_k u_k^l, \quad l = 1, 2, \dots, 2N,$$

and therefore we have a mapping from  $(\rho_k, u_k)$ 's to  $(m_1, m_2, \dots, m_{2N})$ . It has been shown [8] that if the  $\rho_k$ 's are positive and the  $u_k$ 's are distinct, then the mapping is invertible. Therefore, when the number of physical phases  $N$  is finite the system can be closed exactly.

For the examples we will present in Section V we have

$N = 3$ . We define,

$$p_1 = u_1 + u_2 + u_3 \quad (14)$$

$$= \frac{m_6 m_2^2 - m_6 m_3 m_1 + m_5 m_4 m_1 - m_5 m_2 m_3 + m_4 m_3^2 - m_2 m_4^2}{m_5 m_2^2 - m_5 m_3 m_1 + m_4^2 m_1 - 2 m_2 m_3 m_4 + m_3^3}, \quad (15)$$

$$p_2 = u_1 u_2 + u_1 u_3 + u_2 u_3 \quad (16)$$

$$= -\frac{m_6 m_4 m_1 - m_6 m_3 m_2 + m_5 m_3^2 - m_5^2 m_1 + m_5 m_4 m_2 - m_3 m_4^2}{m_5 m_2^2 - m_5 m_3 m_1 + m_4^2 m_1 - 2 m_2 m_3 m_4 + m_3^3} \quad (17)$$

$$p_3 = u_1 u_2 u_3 \quad (18)$$

$$= -\frac{m_6 m_2 m_4 - m_6 m_3^2 - m_5^2 m_2 + 2 m_5 m_4 m_3 - m_5^2 m_2 - m_4^3}{m_5 m_2^2 - m_5 m_3 m_1 + m_4^2 m_1 - 2 m_2 m_3 m_4 + m_3^3}. \quad (19)$$

Then  $m_0$  can be expressed as

$$m_0 = (m_3 - p_1 m_2 + p_2 m_1) / p_3.$$

The first six equations of Eqs. (13) are closed in this manner. For  $N = 2$ , one can define,

$$p_1 = \frac{m_4 m_1 - m_2 m_3}{m_1 m_3 - m_2^2},$$

$$p_2 = \frac{m_2 m_4 - m_3^2}{m_1 m_3 - m_2^2}.$$

Then  $m_0 = (-m_2 + p_1 m_1) / p_2$  and the first four equations are closed. In the case  $N = 1$  the first two equations of the system Eqs. (13) are reduced to the original Euler-Poisson system. One can also define functions,

$$\phi_1 = m_1 m_3 - m_2^2,$$

$$\phi_2 = -m_5 m_2^2 + m_5 m_3 m_1 - m_4^2 m_1 + 2 m_2 m_3 m_4 - m_3^3,$$

as indicators to identify the number of phases at the point  $(z, t)$ . Namely,

$$\# \text{ of phases} = \begin{cases} 1, & \text{if } \phi_1 = 0, \\ 2, & \text{if } \phi_1 > 0, \phi_2 = 0, \\ 3, & \text{if } \phi_2 > 0. \end{cases}$$

To use the multi-phase formulation one must assume a maximum number of phases  $N_{\max}$  at the outset of the calculation, and use indicator functions as above to monitor the actual number of phases  $N$  in the solution [23]. When  $N$  is large one may not get an exact formula for  $m_0$ , but a numerical procedure can be used to obtain  $m_0$  approximately (see Ref. [8]).

#### IV. A LAGRANGIAN APPROACH

For comparison with the new Eulerian method of Section III B and previous work, we next develop a Lagrangian formulation of Eqs. (2).

Upon entering the system at time  $t = t_0$  a fluid element has the coordinates  $(z = 0, t = t_0)$ . The trajectory of the fluid element may be parameterized by either  $(z, t(z, t_0))$  or  $(z(t, t_0), t)$  where the different parameterizations lead to two different sets of equations. Since we consider only cases when the electrons are not reflected, i.e.,  $\partial z / \partial t > 0$ , the inverse function theorem guarantees the equivalence

of the descriptions. In this section we consider the first of the two suggested parameterizations.

We define

$$\begin{cases} z = s, \\ t = t(s, \zeta) \end{cases} \quad (20)$$

with

$$\begin{cases} \frac{\partial t}{\partial s} = \frac{1}{u}, & t(0, \zeta) = \zeta, \\ \frac{\partial u}{\partial s} = \frac{R_{sc} E}{u}, & u(0, \zeta) = u^0(\zeta). \end{cases} \quad (21)$$

By employing the derivative transformations the continuity equation in Lagrangian coordinates becomes

$$\frac{\partial}{\partial s} \left( \rho u \frac{\partial t}{\partial \zeta} \right) = 0.$$

Hence,

$$I(s, \zeta) = \rho u = \frac{\rho^0(\zeta) u^0(\zeta)}{\left| \frac{\partial t}{\partial \zeta} \right|}. \quad (22)$$

The absolute value on the Jacobian  $\partial t / \partial \zeta$  is required by the integral form of mass conservation. For systems that exhibit wave breaking the absolute value is required since the Jacobian changes sign. At the point of wave breaking the Jacobian is zero and the current becomes infinite. At this point Eq. (22) is not valid and an integral equation is required.

In Eulerian coordinates the density is the superposition of each of the densities carried along each of the characteristic curves, i.e.,

$$\rho^E(z, t) = \sum_{\{(s, \zeta): t(s, \zeta) = t, s = z\}} \rho^L(s, \zeta).$$

Gauss' law for  $E$  must account for this superposition. A numerical scheme for solving Eqs. (21) is given in Appendix A.

#### V. NUMERICAL RESULTS

In this section we present results for two cases to test the validity of our formulations. We compare results from the kinetic formulation (Section III A), the multi-phase technique (Section III B), the Lagrangian method (Section IV)—which will serve as the correct reference solution, and the theory of Lau *et al.* [12].

In our examples we consider  $\epsilon(t)$  to be of the form [12]

$$\epsilon(t) = \epsilon_1 \sin(\omega_1 t + \theta_1) + \epsilon_2 \sin(\omega_2 t + \theta_2).$$

The physical parameters and derived quantities used in the examples are listed in Table I.

TABLE I: Physical parameters and derived quantities for a representative klystron design with nominal operating frequency of 1 GHz. The value of  $R_{sc}$  is estimated from Fig. 9-3 in Ref. [14] for a fill factor of  $r_b/a \approx 0.3$  and  $\beta_e r_b \approx 0.1$ . The parameters are chosen so that the results may be compared to those in Ref. [12].

Description	Symbol	Value
beam voltage	$V_0$	8.50 (kV)
beam current	$I_0$	0.25 (A)
beam radius	$r_b$	0.85 (mm)
klystron length	$L = \lambda_q/4$	13.6 (cm)
space charge reduction factor	$R_{sc}$	0.01
dc beam velocity	$u_0 = \sqrt{\frac{2eV_0}{m_e}}$	$5.46 \times 10^7$ (m/s)
dc beam charge density	$\rho_0 = \frac{I_0}{u_0 \pi r_b^2}$	$2.02 \times 10^{-2}$ (C/m <sup>3</sup> )
plasma frequency	$\omega_p = \sqrt{\frac{e\rho_0}{m_e \epsilon_0}}$	$2\pi \times 10^9$ (rad/s)
effective plasma frequency	$\omega_q = \sqrt{R_{sc}\omega_p}$	$2\pi \times 10^8$ (rad/s)
plasma wavelength	$\lambda_p = \frac{2\pi u_0}{\omega_p}$	5.43 (cm)
effective plasma wavelength	$\lambda_q = \frac{\lambda_p}{\sqrt{R_{sc}}}$	54.3 (cm)

### A. Multi-phase, kinetic, and Lagrangian schemes

For comparison of the multi-phase, kinetic, and Lagrangian schemes we choose the velocity modulation function  $\epsilon(t)$

$$\epsilon(t) = \epsilon_1 \sin(\omega_1 T t), \quad (23)$$

with  $\omega_1 = 2\pi \times 10^9$  (rad/s) and  $\epsilon_1 = 0.4$  (i.e.,  $\epsilon_2 = 0$ ).

We first show the numerical solutions obtained by integrating the Euler-Poisson equations (2) without accounting for multiple phases [Eqs. (13) with  $N_{\max} = 1$ ]. In Fig. 3 we plot the current  $I(z, t)$  solutions at different locations. The solution first develops a single peak and is then smoothed out by the potential. This solution does not allow “overtaking” and thus is not physically correct [compare with Fig. 4].

The current waveforms at  $z = 1.0$  predicted by the methods presented in this paper are shown in Fig. 4. The methods include solving directly the Vlasov-Poisson system with  $\Delta z = 5 \times 10^{-5}$ ,  $\Delta t = 4\Delta z$ ,  $\Delta v = \Delta z$ , solving the moment system with  $\Delta z = 5 \times 10^{-3}$ ,  $\Delta t = 2\Delta z$ , and solving the Lagrangian equations with  $\Delta z = 5 \times 10^{-3}$ ,  $\Delta t = 2\Delta z$  via the method developed in Appendix A. Using the analysis of Section VI we determined that there are three phases in the multi-phase region.

The numerical computations of the current display similar structure. However, the Eulerian methods – both the kinetic and the moment methods – display smooth transitions across phase boundaries, whereas the Lagrangian method shows discontinuous transitions. The discrepancy lies in the fact that the Eulerian methods use numerical viscosity, which smears out the discontinuity as in any standard shock capturing scheme. In the kinetic

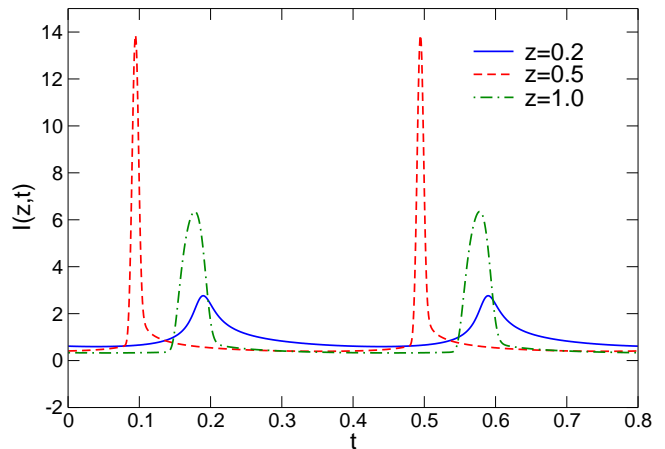


FIG. 3: The current solutions at different locations obtained from the Euler-Poisson system when only accounting for a single phase in the solution (i.e.,  $N_{\max} = 1$ ). The solutions are displayed for two periods:  $t \in (0, 0.8]$ .

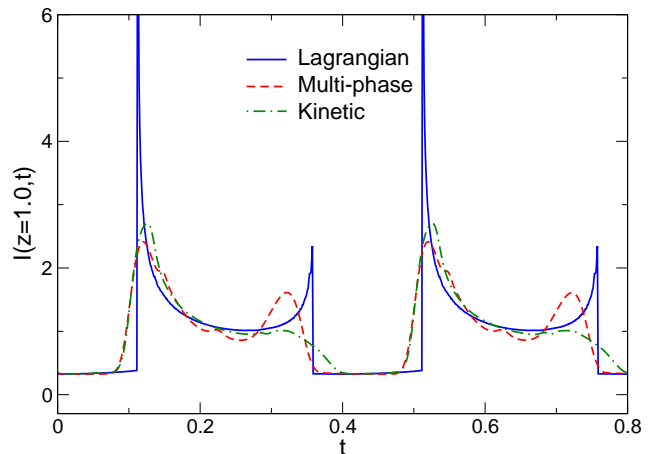


FIG. 4: The current waveforms at  $z = 1.0$  predicted by the kinetic formulation, the multi-phase formulation, and the Lagrangian formulation. The solutions are displayed for two periods:  $t \in (0, 0.8]$ .

computation, a narrow Gaussian is used to represent the delta function boundary data, as described in Appendix A, which could further smooth out the discontinuity. The peaks in the current waveform are theoretically of infinite height; however, due to numerical resolution of the methods they have finite amplitudes in the Eulerian solutions.

To further illustrate the existence of the multi-valued solutions in Eulerian coordinates, we plot the multi-valued velocity profile  $(u_1, u_2, u_3)$  obtained from the moment system (13) together with the algebraic equations (14)–(19), as well as the Lagrangian solutions in Figs. 5(a)–5(c). The velocities produced by these two methods are in good agreement, and the large multi-phase region of the velocity solution is clearly evident.

As the number of phases change  $u_1$  (or  $u_3$ ) and  $u_2$  approach each other and the system (14)–(19) becomes ill-conditioned. This fact accounts for the jumps in  $u_3$  at the phase boundary seen in Figs. 5(a)–5(c). This is of little concern since the values at the jump are disregarded, as in any shock computation.

Among the three numerical methods, the multi-phase method is the most computationally efficient. For  $N$  grid points in the  $z$  and  $t$  directions the computational complexity is of order  $O(N^2)$  for the multi-phase method. Solving the kinetic Vlasov-Poisson equations by finite difference methods are often  $O(N^3)$  because of the additional phase-space dimension. Another difficulty in solving the kinetic equation is due to the irregularity of the solution, i.e., the presence of delta functions. Although one can replace delta functions by smoother functions, such as Gaussian distributions with narrow width, the numerical grid size must decrease as the width decreases. The development of an efficient coupling of the moment system and the kinetic equations is currently in progress. The Lagrangian method, along with the Finite Fourier method, offers the best resolution for a given mesh size. However, the evaluation of the Fourier integrals can lead to  $O(M \times N^2)$  cost, where  $M$  is the number of Fourier modes. In fact, for the test problem in Section VB2, the Lagrangian method takes several days to finish on a 1.8 GHz Gnu/Linux machine, while solving the moment system only takes several minutes. In addition, because of the presence of the peaks a very large number of modes are required to represent the solutions. Therefore, the numerical solution  $I(z, t)$  often displays spurious oscillations. Interestingly, since the trajectory  $\hat{t}(z)$  is well resolved in the Lagrangian method, it is preferable to use Eq. (22) to compute the current once the trajectory is obtained. A natural fix to speed up the Lagrangian method would be to use a local basis in lieu of a Fourier representation.

## B. Comparison to existing theory

The klystron theory of Lau *et al.* [12] has been favorably compared to certain experimental results for several cases [19, 20]. Therefore, it is useful to compare results from the methods in this paper to those in Ref. [12]. It is important to note that in Refs. [19, 20] a direct experimental measurement of the time-dependent current waveform was not available. Consequently, simulation and experimental measurement comparisons were restricted to comparisons of measured and predicted spectra of the output RF signal. Moreover, in Refs. [19, 20], the number of phases in the solutions were not quantified. As shown in this and the following section, the extent of multi-phase may have a strong effect on how well a theory will match the measurements. In this section we compare results from the various methods for two cases. The first case represents a relatively strong input modulation with  $\epsilon_1 = 0.4$ , the same case that was analyzed

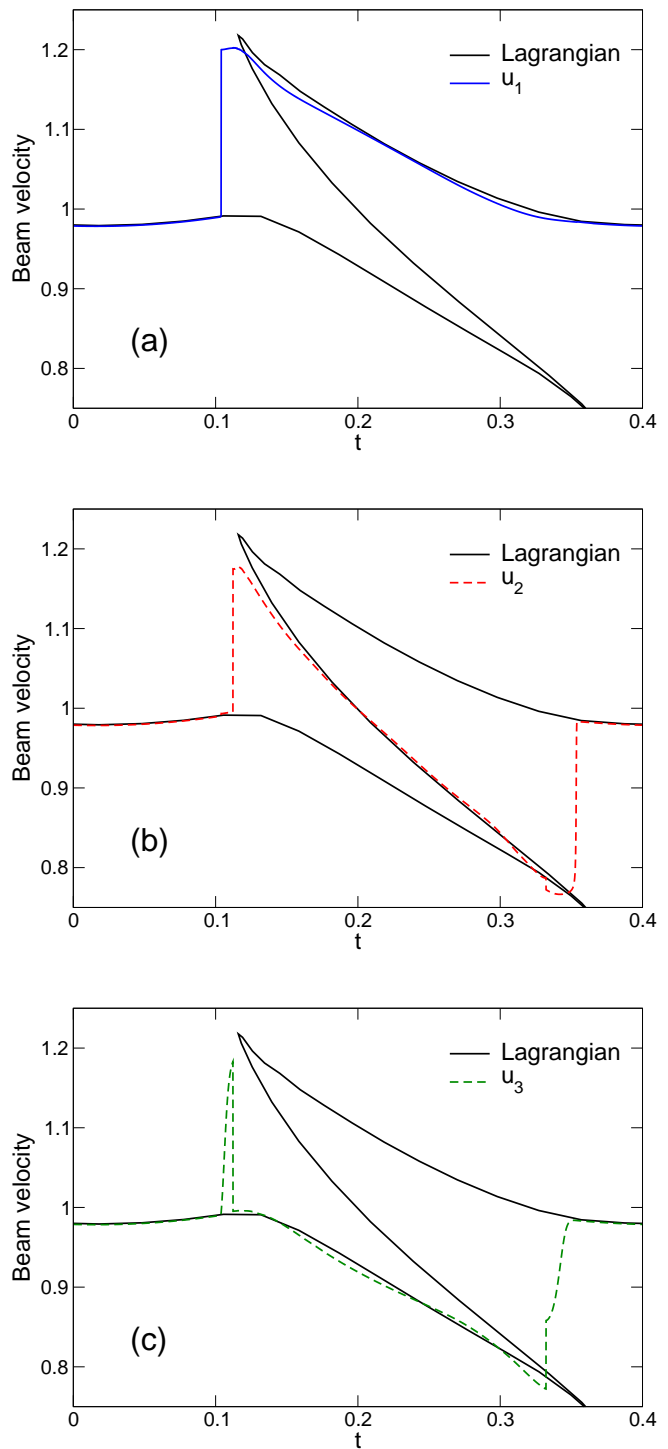


FIG. 5: The multi-valued velocity profile (a)  $u_1$ , (b)  $u_2$ , and (c)  $u_3$  and the Lagrangian velocity solution at location  $z = 1.0$ . The solutions are displayed for one period:  $t \in (0, 0.4]$ . The Lagrangian solution  $(\hat{t}, \hat{v})$  has been converted into this interval using the periodic properties of the solution.

in Section V A. As shown later, the solution to this case has a significant amount of multi-phase, and therefore differences may be expected in the predictions of differing models, depending on what factors limit the accuracy of the individual models. For this case, we directly compare the complete time-varying beam current, in contrast to the radiation spectrum basis of comparison used between simulation and experiment in Refs. [19, 20]. We have observed that this time-varying current is a sensitive indicator of the accuracy of a model at capturing multi-phase characteristics. The second comparison represents a case where the input signal contains two frequencies,  $\omega_1$  and  $\omega_2$  which is the same basis of model-to-experiment comparison used in Refs. [19, 20]. Moreover, in this case we select a comparatively weak input modulation, with  $\epsilon_1 = \epsilon_2 = 0.1$ , identical to the conditions used in the simulation-experiment comparisons of Refs. [19, 20]. Finally, as done in Refs. [19, 20], we adopt the output radiation spectrum as the basis of comparison. In this case, we show that it is not possible to discern differences between different model solutions or between model and experimental measurements. In Section VI, we will show that this is a direct result of the fact that for these conditions, the extent of multi-phase is very small, so that comparisons or validations for these conditions are not particularly discriminating.

### 1. Single frequency input

First we consider again the example of Section V A. In Fig. 6 we compare the output current computed by the analytic solution of Ref. [12] and the Lagrangian method of this paper. The analytic solution of Lau *et al.* is seen to deviate from the Lagrangian method in that it has narrower multi-phase zones.

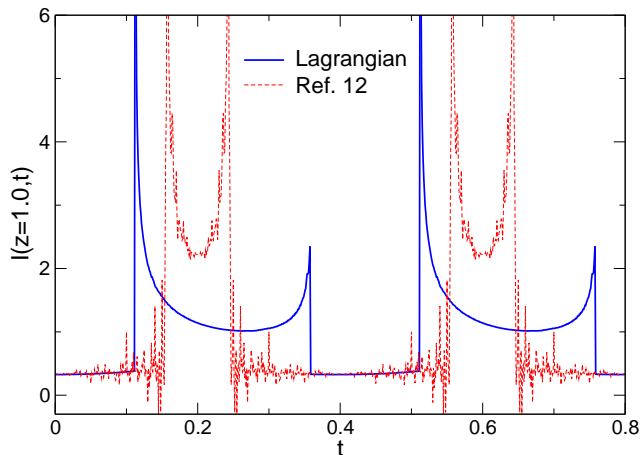


FIG. 6: The current waveforms at  $z = 1.0$  predicted by the Lagrangian formulation and Eq. (C6) of Ref. [12]. The solutions are displayed for two periods:  $t \in (0, 0.8]$ .

For an alternate view of the discrepancies in Fig. 6 we compare characteristic curves from the analytic solution

in Eq. (B17) to those computed by numerical solution of the Lagrangian system in Fig. 7. One can see that the deviation of the solutions becomes substantial after characteristics have crossed (about  $z = 0.5$ ). For these parameters the characteristics predicted by Eq. (B17) versus those predicted by the theory of Ref. [12] [repeated in Eq. (B16) of the present paper] are indistinguishable. However, neither Eq. (B17), Eq. (B16), nor the result of Ref. [12] are valid beyond wave breaking since they do not account for the absolute value of the Jacobian in the denominator of Eq. (B3).

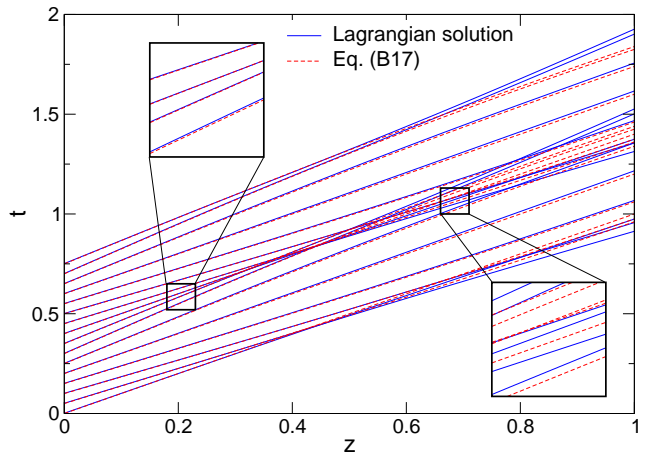


FIG. 7: Two periods of characteristic curves (arrival time as a function of position) predicted by numerical solution of the Lagrangian formulation (Section A 2) and the analytic formula in Eq. (B17). The characteristics in the magnified boxes illustrate that the characteristic curves of the Lagrangian simulation and the analytic theory agree prior to wave breaking (prior to crossing characteristics), but deviate after wave breaking (after characteristics have crossed).

To further contrast our results to that of Ref. [12], we provide here details of where Ref. [12] is in error. As mentioned above the error of Ref. [12] is the neglect of an absolute value sign on the Jacobian in the Lagrangian continuity equation. In particular, in Appendix A of Ref. [12] the Lagrangian continuity equation Eq. (L-A6) (for clarity equation numbers from Ref. [12] will be preceded by an “L”) does not have the absolute value sign on the Jacobian [compare Eq. (L-A6) to Eq. (B3) of the present paper]. It is precisely this fact that allows for the derivation of the harmonic oscillator equation for the beam displacement, Eq. (L-A13), and the analytic results which follow, e.g., the beam displacement function (L-5) and the beam current (L-C6). Since our numerical solution to the Lagrangian equations accounts for the absolute value when computing the characteristics we claim that it is the correct solution to the Euler-Poisson equations when the solution becomes multi-valued. Note that the ballistic limit ( $\omega_p = 0$ ) of the theory in Ref. [12] [e.g. Eq. (L-C6)] is correct since in this case the absolute value sign does not enter into the calculation of the characteristics.

Another publication by the same authors [21] considers explicitly the issue of electron overtaking. It is important to note that we agree with all of the calculations performed in Ref. [21]. However, the choice of Eq. (7) in Ref. [21] as the equation determining the beam characteristics *when accounting for space charge* again implicitly neglects the absolute value sign from the Jacobian as described above.

Lastly, in Appendix B of the present paper we describe a calculation that is very similar to the calculations in Appendix A of Ref. [12]. In this calculation we too omit the absolute value sign in order to make analytic progress that is valid prior to wave breaking. In our calculations we find additional terms that were neglected in Ref. [12]. However, for the parameters in this section these additional terms appear to be very small, i.e., the characteristics predicted by Eq. (B16) and Eq. (B17) are indistinguishable.

## 2. Two frequency input

A case of considerable interest in klystrons is when the input signal contains more than one frequency. For such an input signal the electron beam nonlinearity produces additional spectral components (so called intermodulation products) in the beam modulation, and hence in the RF output signal. For such input modulations the theory of Lau *et al.* [12] has been compared to experiments with remarkable agreement [19, 20]. We test our formulations on such an input spectrum and compare our results to those computed in Ref. [12].

We have the velocity modulation function  $\epsilon(t)$

$$\epsilon(t) = \epsilon_1 \sin(\omega_1 T t) + \epsilon_2 \sin(\omega_2 T t), \quad (24)$$

with  $\epsilon_1 = \epsilon_2 = 0.1$ ,  $\omega_1 = 2\pi 1.003 \times 10^9 \text{ rad/s}$ ,  $\omega_2 = 2\pi 1.007 \times 10^9 \text{ rad/s}$ . The beam spectrum at  $z = 1.0$  is shown in Fig. 8. The spectral components are the Fourier coefficients of the current at  $z = 1.0$ , computed from the multi-phase equations.

The fact that the two predictions shown in Fig. 8 agree so well is due to the fact the multi-phase region for this case is very small. In Section VI we provide a method for quantifying the size of the multi-phase region, and show that it is very small for this case. We did not compute an analogous case with a large  $\epsilon_1$  since the benchmark Lagrangian solution, with its current numerical implementation, is prohibitively expensive for these frequency spacings.

## VI. BREAKING TIME AND LOCATION

In this section we develop tools for studying wave breaking time and location based on the alternative Lagrangian formulation given in Appendix B. This is of relevance as one chooses the physical parameters as well

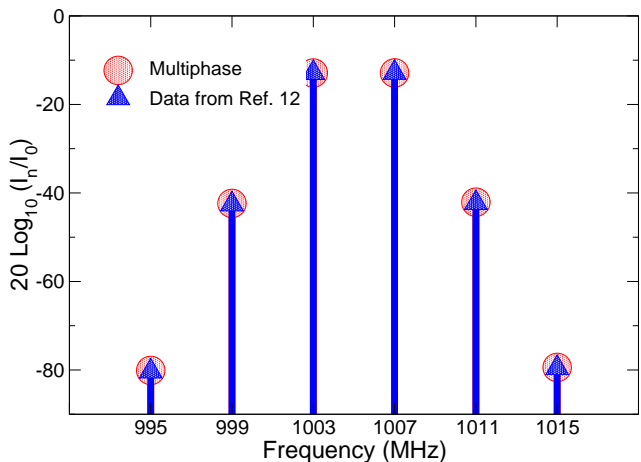


FIG. 8: Output spectrum due to input modulation in Eq. (24). Included are the third order (999, 1011) and fifth order (995, 1015) intermodulation products. Shown are results from the multi-phase formulation and data from Ref. [12].

as the computational domain to observe multi-phase phenomena. Similar results are obtained in Ref. [11] for initial value problems.

In Appendix B we derive the following expression for the Jacobian of the alternate Lagrangian coordinates [Eq. (B14)]

$$\frac{\partial z}{\partial \zeta} = \frac{1}{\sqrt{\hat{R}_{sc}}} \frac{d}{d\zeta} u^0(\zeta) \sin \sqrt{\hat{R}_{sc}} (\tau - \zeta) - u^0(\zeta)$$

which is only valid *prior to wave breaking*. To find the critical time at which the solution breaks, we set  $\partial z / \partial \zeta$  equal to zero

$$\sqrt{\hat{R}_{sc}} \frac{u^0(\zeta)}{\frac{d}{d\zeta} u^0(\zeta)} = \sin \sqrt{\hat{R}_{sc}} (\tau - \zeta), \quad (25)$$

and determine conditions for which Eq. (25) has solutions. Equation (25) is solvable as long as the value of left hand side is between  $-1$  and  $1$ .

For the case of a modulation with a single frequency Eq. (25) becomes

$$\sin \sqrt{\hat{R}_{sc}} (\tau - \zeta) = \frac{2\sqrt{\hat{R}_{sc}}}{\epsilon_1 \omega_1} \frac{1 + \frac{\epsilon_1}{2} \sin(\omega_1 \zeta)}{\cos(\omega_1 \zeta)}. \quad (26)$$

Since for  $\epsilon_1 \leq 2$

$$\min_{\zeta} \frac{1 + \frac{1}{2} \epsilon_1 \sin(\omega_1 \zeta)}{|\cos(\omega_1 \zeta)|} = \sqrt{1 - \frac{\epsilon_1^2}{4}},$$

a necessary condition for Eq. (26) to have solutions is

$$\frac{\omega_1 \epsilon_1}{2\sqrt{\hat{R}_{sc}}} \geq \sqrt{1 - \frac{\epsilon_1^2}{4}}. \quad (27)$$

If Eq. (26) is satisfied, then at least two characteristic curves will cross at time  $\tau$ . The multiple values of  $\zeta$  can

be solved from Eq. (26). These calculations can also be carried out for the general boundary condition given in Eq. (4).

A direct way to see whether a solution is multi-valued is to plot the left hand side of Eq. (25). For parameters where the value is between  $-1$  and  $1$  multi-phase phenomena is ensured. For the parameters of Sections V A and V B 1 the left hand side of Eq. (25) is shown in Fig. 9. Since the left hand side takes values between  $-1$  and  $1$  the solutions become multi-valued in part of the domain. One can show using Eq. (26) that for these parameters the number of phases in the multi-phase solution is three.

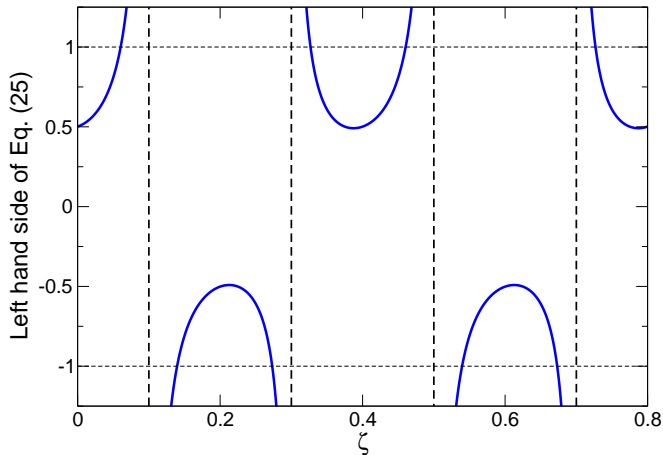


FIG. 9: The left hand side of Eq. (25) illustrating multi-phase content in the current waveform. The fluid elements labeled by  $\zeta$  where the left hand side of Eq. (25) is between  $-1$  and  $1$  will enter the multi-phase region.

For the parameters of Section V B 2 we plot the left hand side of Eq. (25) in Fig. 10. This illustrates that for these parameters the solutions are multi-valued. However, the multi-valued regions are tiny, which may illustrate why our numerical results, unlike the single frequency input example, agree with the data of Lau *et al.*

## VII. CONCLUSIONS

In this paper, we develop an Eulerian technique to simulate multi-phase phenomena for electron beam wave breaking in a modulated electron beam. The basic physical model is the Euler-Poisson system. We provide three methods of solving the Euler-Poisson system (2) that are valid when the solutions are multi-valued: a kinetic formulation, a multi-phase Eulerian formulation, and a Lagrangian formulation. We compare the methods with each other and with the analytic theory of Ref. [12] for a modulated electron beam. For the case when the input modulation contains a single frequency, the three methods are seen to agree with each other, while differing somewhat from the analytic theory in Ref. [12]. The

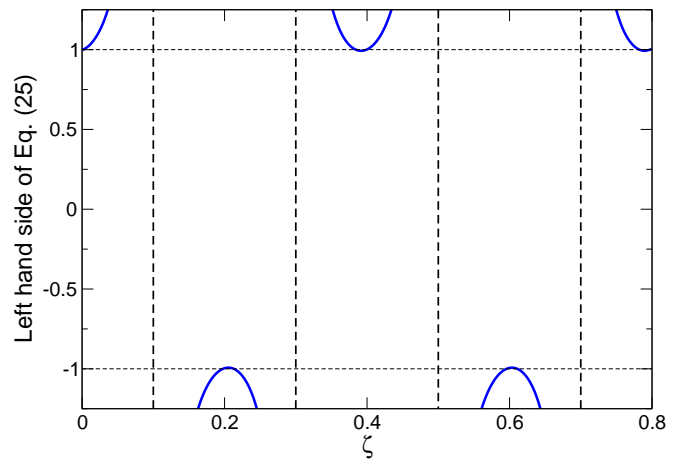


FIG. 10: The left hand side of Eq. (25) for two frequency input. The figure illustrates that there is multi-phase content in the current waveform. The fluid elements labeled by  $\zeta$  where the left hand side of Eq. (25) is between  $-1$  and  $1$  will enter the multi-phase region.

multi-valued structure of the current is confirmed by the multi-phase Eulerian technique as well as the Lagrangian technique. For an input modulation with two frequencies the output current spectrum is computed. In this case the multi-valued region is almost negligible, and the multi-phase method is in agreement with the theory of Ref. [12].

## VIII. ACKNOWLEDGMENTS

X.T. Li gratefully acknowledges support in part by ONR Grant N00014-01-1-0674.

J.G. Wöhlbier and J.H. Booske gratefully acknowledge support in part by AFOSR Grant 49620-00-1-0088 and by DUSD (S&T) under the Innovative Microwave Vacuum Electronics Multidisciplinary University Research Initiative (MURI) program, managed by the United States Air Force Office of Scientific Research under Grant F49620-99-1-0297.

S. Jin gratefully acknowledges support in part by the National Science Foundation, Grant DMS-0196106.

## APPENDIX A: NUMERICAL SCHEMES

### 1. Kinetic scheme for the multi-phase system

In this section we briefly present the numerical methods we use to solve the multi-phase system (13). The schemes are called kinetic schemes, which were developed in Ref. [8] for multi-phase moment equations. The method consists of a transport step through the kinetic equation and a projection into the equilibrium state in Eq. (11). See Ref. [8] for details.

We first give a direct scheme to solve the kinetic equation, and this scheme will induce a “kinetic scheme” for the moment system. Since we restrict our phase variable  $v$  to be positive, we can simply use upwind scheme to solve the kinetic equation,

$$\frac{w_{j,k}^n - w_{j,k}^{n-1}}{\Delta t} + v_k \frac{w_{j+1,k}^n - w_{j,k}^n}{\Delta z} + \hat{R}_{sc} E_j^n w_v = 0. \quad (\text{A1})$$

Here  $w_{j,k}^n = w(z_j, v_k, t_n)$ . Note that since we update the solution values in the  $z$  direction, the upwind difference is done in the  $t$  derivative. The discretization of the  $v$  derivative depends on the sign of  $E$ . For instance, one may use,

$$w_v = \begin{cases} \frac{w_{j,k}^n - w_{j,k-1}^n}{\Delta v}, & \text{if } E_j^n > 0, \\ \frac{w_{j,k+1}^n - w_{j,k}^n}{\Delta v}, & \text{if } E_j^n \leq 0. \end{cases}$$

The electric field  $E_j^n$  can be obtained by simple finite difference, for example,

$$\frac{E_{j+1}^n - E_j^n}{\Delta z} = \rho_j^n.$$

To improve the accuracy of the above schemes non-oscillatory second order schemes can be introduced following Ref. [8].

Because of the presence of delta functions in the solution, we need to smooth out the singularities in order for the point-wise values to make sense. In practice, a Gaussian distribution is usually used. For example, the boundary condition (6) can be replaced by,

$$w(0, v, t) = \rho^0(t) \exp^{-(v-u^0(t))^2/\epsilon} / \sqrt{2\pi\epsilon},$$

with  $\epsilon$  as a small parameter. We also take the grid size to be smaller than  $\epsilon$  to resolve the small width. For this reason, particle methods, which are similar to our Lagrangian method, are suitable for the problem. We have found that a particle method offers a substantial advantage over solving the kinetic equation by finite differencing, but is still four to five times more expensive than our Lagrangian method. For example, for the problem of Section V B 2 the Lagrangian method requires several days of computation, the particle method requires more than ten days of computation, and solving the kinetic equation by finite differencing requires about four weeks of computation on a 1.8 GHz Gnu/Linux PC. Since our purpose of solving the kinetic equation is to numerically verify the multi-phase approach, we will not discuss this issue further.

In order to get a numerical method for the moment system, one can simply integrate (A1) with respect to  $v$  and use the closure ansatz (III B). Since all of the waves are going to the right in the context of the klystron, the kinetic scheme is reduced to an upwind procedure. Namely,

$$\frac{m_l(z_k, t_n) - m_l(z_k, t_{n-1})}{\Delta t} + \frac{m_{l+1}(z_{k+1}, t_n) - m_{l+1}(z_k, t_n)}{\Delta x} = (l-1)\hat{R}_{sc} m_{l-1}(z_k, t_n) E(z_k, t_n),$$

where  $\delta_n = 1$  if  $n = 0$  and 0 otherwise. Notice that (A2)  $\tilde{E}_0 \equiv 0$ .

for  $l = 0, 1, \dots$ . The potential is obtained from integration of  $m_0$ . Periodic conditions are imposed in the  $t$  direction and the numerical methods can be advanced in the  $z$  direction up to  $z = L$ .

## 2. Finite difference scheme for the Lagrangian system

In this section, we present a numerical procedure that solves the Lagrangian equations (21). The novelty of this approach is that one can easily switch to Eulerian coordinates to solve the electric field  $E(z, t)$ .

First we define the characteristic curves of the Euler-Poisson system,  $(\hat{z}, \hat{t}(t_0; s), \hat{v}(t_0; s))$ ,

$$\begin{cases} \frac{d}{ds} \hat{t} = 1/\hat{v}, & t = t_0 \text{ at } s = 0, \\ \frac{d}{ds} \hat{v} = \hat{R}_{sc} E/\hat{v}, & v = u^0(t_0) \text{ at } s = 0, \\ \hat{z} = s. \end{cases} \quad (\text{A3})$$

Equations (7) may be projected to Eqs. (A3) by forcing  $v_0 = u^0(t_0)$ . This fact will be used in the following computation. Notice that Eqs. (A3) are the same as Eqs. (20) and (21); however, we use a different notation here to make the connection between Eqs. (A3) and Eqs. (7).

The characteristic curves of Euler-Poisson system may experience crossing which indicates the appearance of multi-phase solutions as we have seen in Section VI. However the bicharacteristic curves of the kinetic equation (5) will never cross since the Jacobian of Eq. 9 is always non-zero. This is essentially why the kinetic approach is capable of unfolding the multi-valued solutions.

Secondly we represent the density  $\rho(z, t)$  in Eulerian coordinates by a Fourier series,

$$\rho(z, t) = \sum_n \tilde{\rho}_n(z) e^{i\omega_0 n t}. \quad (\text{A4})$$

The coefficients  $\tilde{\rho}_n$  can be determined by the integral,

$$\tilde{\rho}_n = \frac{\omega_0}{2\pi} \int_0^{2\pi/\omega_0} e^{-i\omega_0 n t} \rho(z, t) dt.$$

The electric field can also be represented by a Fourier series,

$$E(z, t) = \sum_n \tilde{E}_n(z) e^{i\omega_0 n t}, \quad (\text{A5})$$

and

$$\frac{\partial \tilde{E}_n}{\partial z}(z) = \tilde{\rho}_n(z) - \delta_n, \quad (\text{A6})$$

We now derive a formula to compute these Fourier coefficients with the aid of the kinetic distribution  $w(z, v, t)$ ,

$$\begin{aligned}
\tilde{\rho}_n &= \frac{\omega_0}{2\pi} \int_0^{\frac{2\pi}{\omega_0}} \int_{\mathbb{R}^+} e^{-i\omega_0 n t} w(z, v, t) dv dt \\
&= \frac{\omega_0}{2\pi} \int_0^{\frac{2\pi}{\omega_0}} \int_{\mathbb{R}^+} e^{-in\omega_0 t(v_0, t_0; z)} w(0, v_0, t_0) \Delta dv_0 dt_0 \\
&= \frac{\omega_0}{2\pi} \int_0^{\frac{2\pi}{\omega_0}} \int_{\mathbb{R}^+} e^{-in\omega_0 t(v_0, t_0; z)} \rho^0 \delta(v_0 - u^0(t_0)) \Delta dv_0 dt_0, \\
&= \frac{\omega_0}{2\pi} \int_0^{\frac{2\pi}{\omega_0}} e^{-in\omega_0 \hat{t}(t_0; z)} I^0(t_0) / \hat{v}(t_0; z) dt_0 \quad (\text{A7})
\end{aligned}$$

In the above computations we made a transformation from  $(v, t)$  coordinates to  $(v_0, t_0)$  coordinates using the Jacobian in Eq. (9), we have used the projection from Eqs. (7) to Eqs. (A3) which is realized by the delta function, and we have used the fact that the initial current  $I^0(t_0) = \rho^0(t_0)u^0(t_0)$ .

Finally we can build a numerical procedure. Within one loop  $t \in [z, z + \Delta z)$  we use a second order Runge Kutta method,

1. solve (A3) for a half step,

$$\begin{aligned}
\hat{t}(t_0, z + \frac{1}{2}\Delta z) &= \hat{t}(t_0; z) + \frac{1}{2}\Delta z / \hat{v}(t_0; z), \\
\hat{v}(t_0, z + \frac{1}{2}\Delta z) &= \hat{v}(t_0; z) + \frac{1}{2}\Delta z \hat{R}_{sc} E(\hat{t}(t_0; z), z) / \hat{v}(t_0; z),
\end{aligned}$$

2. use the formula (A7) and trapezoidal quadrature to compute  $\tilde{\rho}_n(z)$ ,

$$3. \tilde{E}_n(z + \frac{1}{2}\Delta z) = \tilde{E}_n(z) + \frac{1}{2}\Delta z (\tilde{\rho}_n(t, z) - \delta_n),$$

4. use fast Fourier transform to compute  $E(\hat{t}(t_0; z + \frac{1}{2}\Delta z), z + \frac{1}{2}\Delta z)$  by (A5),

5. solve (A3) for the whole step,

$$\begin{aligned}
\hat{t}(t_0, z + \Delta z) &= \hat{t}(t_0; z) + \Delta z / \hat{v}(t_0; z + \frac{1}{2}\Delta z), \\
\hat{v}(t_0, z + \Delta z) &= \hat{v}(t_0; z) \\
&\quad + \Delta t \hat{R}_{sc} E(\hat{t}(t_0; z + \frac{1}{2}\Delta z), z + \frac{1}{2}\Delta z) / \hat{v}(t_0; z + \frac{1}{2}\Delta z),
\end{aligned}$$

6. compute  $E(\hat{t}(t_0; z + \Delta z), z + \Delta z)$  as in previous steps,

7.  $z = z + \Delta z$ , go to 1 unless  $z = L$ .

**Remark 1:** The technique used in Eq. (A7) can be easily applied to other quantities. For example, one can make use of Fourier series and obtain the Fourier coefficients of the current,

$$\begin{aligned}
\tilde{I}_1(L, n) &= \frac{\omega_0}{2\pi} \int_0^{2\pi/\omega_0} e^{-in\omega_0 t} m_1(L, t) dt \quad (\text{A8}) \\
&= \frac{\omega_0}{2\pi} \int_0^{2\pi/\omega_0} e^{-in\omega_0 \hat{t}(t_0; L)} I(0, t_0) dt_0, \quad (\text{A9})
\end{aligned}$$

which has appeared in Ref. [12].

**Remark 2:** By replacing the Fourier mode in Eq. (A4) with a delta distribution  $\delta(t - t_n)$ , with  $t_n$  as discrete points on the  $t$  axis, one obtains the traditional particle method. We have found that the Fourier method has better performance than the particle method (see previous section).

## APPENDIX B: ALTERNATIVE LAGRANGIAN COORDINATES

Next we introduce an alternative set of Lagrangian coordinates. The resulting Lagrangian equations can be analytically solved, where the solutions are only valid prior to wave breaking. The resulting formulas allow us to compute breaking times and locations.

Define the Lagrangian coordinates  $(\tau, \zeta)$  which are connected to the Eulerian independent variables  $(z, t)$  by

$$\begin{cases} z = z(\tau, \zeta) \\ t = \tau \end{cases} \quad (\text{B1})$$

with

$$\begin{cases} \frac{\partial z}{\partial \tau} = u, & z(\zeta, \zeta) = 0 \\ \frac{\partial u}{\partial \tau} = \hat{R}_{sc} E, & u(0, \zeta) = u^0(\zeta). \end{cases} \quad (\text{B2})$$

By the definitions in Eq. (B1) and Eq. (B2) the Lagrangian coordinates  $(\tau, \zeta)$  are equivalent to the Lagrangian coordinates  $(t, t_0)$  that one often sees in the microwave device literature [12].

Using Eq. (B1) and Eq. (B2) one finds that the continuity equation in these Lagrangian coordinates is

$$\frac{\partial}{\partial \tau} \left( \frac{\partial z}{\partial \zeta} \rho \right) = 0$$

which considering the boundary data has the solution

$$\rho(\tau, \zeta) = \frac{\rho^0(\zeta)u^0(\zeta)}{\left| \frac{\partial z}{\partial \zeta} \right|} \quad (\text{B3})$$

where the absolute value sign on the Jacobian is required by the integral form of mass conservation.

This Lagrangian formulation can be analytically solved, but the solution only holds prior to wave breaking. We consider the case when the Jacobian is negative definite and we remove absolute value signs. For the Euler-Poisson system in these Lagrangian coordinates we have

$$\frac{\partial^2 z}{\partial \tau^2} = \hat{R}_{sc} E \quad (\text{B4})$$

$$\rho \frac{\partial z}{\partial \zeta} = -\rho^0(\zeta)u^0(\zeta) \quad (\text{B5})$$

$$\frac{\partial E}{\partial \zeta} = \frac{\partial z}{\partial \zeta} (\rho - 1). \quad (\text{B6})$$

Define

$$X \equiv \frac{\partial z}{\partial \zeta}(\rho - 1) \quad (\text{B7})$$

and use (B4)–(B6) to get

$$\frac{\partial^2 X}{\partial \tau^2} + \hat{R}_{\text{sc}} X = 0. \quad (\text{B8})$$

The first of the two initial conditions required to solve Eq. (B8) is

$$X(\zeta, \zeta) = u^0(1 - \rho^0). \quad (\text{B9})$$

Then notice that

$$\frac{\partial X}{\partial \tau}(\zeta, \zeta) = -\frac{\partial u}{\partial \zeta}(\zeta, \zeta) \quad (\text{B10})$$

and compute

$$\frac{\partial u}{\partial \xi}(\tau(\xi), \zeta(\xi)) = \frac{\partial u}{\partial \tau} \frac{\partial \tau}{\partial \xi} + \frac{\partial u}{\partial \zeta} \frac{\partial \zeta}{\partial \xi} \quad (\text{B11})$$

on  $(\tau, \zeta) = (\xi, \xi)$ . Since  $u(\zeta, \zeta) = u^0(\zeta)$  and  $E(\zeta, \zeta) = E^0(\zeta)$  one gets

$$\frac{\partial u}{\partial \zeta}(\tau, \zeta) = \hat{R}_{\text{sc}} E^0(\zeta) + \frac{du^0}{d\zeta}(\zeta), \quad \text{on } \tau = \zeta,$$

so

$$\frac{\partial X}{\partial \tau}(\zeta, \zeta) = -\hat{R}_{\text{sc}} E^0(\zeta) - \frac{du^0}{d\zeta}(\zeta). \quad (\text{B12})$$

Finally, solving Eq. (B8) subject to the initial conditions one has

$$X(\tau, \zeta) = u^0(1 - \rho^0) \cos \sqrt{\hat{R}_{\text{sc}}}(\tau - \zeta) - \frac{1}{\sqrt{\hat{R}_{\text{sc}}}} \left[ \hat{R}_{\text{sc}} E^0 + \frac{du^0}{d\zeta} \right] \sin \sqrt{\hat{R}_{\text{sc}}}(\tau - \zeta). \quad (\text{B13})$$

In the remainder of the calculation we consider a uniform input density so  $\rho^0 = 1$  and  $E^0 = 0$ , and we get the following expression for the Jacobian

$$\frac{\partial z}{\partial \zeta} = \frac{1}{\sqrt{\hat{R}_{\text{sc}}}} \frac{du^0}{d\zeta}(\zeta) \sin \sqrt{\hat{R}_{\text{sc}}}(\tau - \zeta) - u^0(\zeta). \quad (\text{B14})$$

The analytic solvability of Eq. (B14) depends on  $u^0(\zeta)$ .

For the boundary data in Eq. (4), repeated here

$$u^0(\zeta) = 1 + \frac{1}{2} \sum_n \epsilon_n \sin(\omega_n \zeta + \theta_n)$$

with the  $\omega_n$  normalized frequencies one gets

$$z(\tau, \zeta) = \tau - \zeta + \sum_n \frac{\epsilon_n \omega_n}{2\sqrt{\hat{R}_{\text{sc}}}} \left\{ \frac{\cos \left[ (\omega_n - \sqrt{\hat{R}_{\text{sc}}}) \zeta + \sqrt{\hat{R}_{\text{sc}}}\tau + \theta_n \right]}{2(\sqrt{\hat{R}_{\text{sc}}} - \omega_n)} + \frac{\cos \left[ (\omega_n + \sqrt{\hat{R}_{\text{sc}}}) \zeta - \sqrt{\hat{R}_{\text{sc}}}\tau + \theta_n \right]}{2(\sqrt{\hat{R}_{\text{sc}}} + \omega_n)} - \frac{\sqrt{\hat{R}_{\text{sc}}} \cos(\omega_n \tau + \theta_n)}{\hat{R}_{\text{sc}} - \omega_n^2} \right\} + \frac{1}{2} \sum_n \frac{\epsilon_n}{\omega_n} [\cos(\omega_n \zeta + \theta_n) - \cos(\omega_n \tau + \theta_n)]. \quad (\text{B15})$$

The theory of Ref. [12] gives for the position function of a fluid element when  $\epsilon(\zeta) = \epsilon_1 \sin(\omega_1 \zeta)$  [24]

$$z(\tau, \zeta) = \tau - \zeta + \frac{\epsilon_1}{2\omega_p} \sin(\omega_1 \zeta) \sin(\omega_p(\tau - \zeta)) \quad (\text{B16})$$

where we have introduced our notation and normalizations. Alternatively Eq. (B15) gives

$$z(\tau, \zeta) = \tau - \zeta + \frac{\epsilon_1 \omega_1}{2\sqrt{\hat{R}_{\text{sc}}}} \left\{ \frac{\cos \left[ (\omega_1 - \sqrt{\hat{R}_{\text{sc}}}) \zeta + \sqrt{\hat{R}_{\text{sc}}}\tau \right]}{2(\sqrt{\hat{R}_{\text{sc}}} - \omega_1)} + \frac{\cos \left[ (\omega_1 + \sqrt{\hat{R}_{\text{sc}}}) \zeta - \sqrt{\hat{R}_{\text{sc}}}\tau \right]}{2(\sqrt{\hat{R}_{\text{sc}}} + \omega_1)} - \frac{\sqrt{\hat{R}_{\text{sc}}} \cos(\omega_1 \tau)}{\hat{R}_{\text{sc}} - \omega_1^2} \right\} + \frac{1}{2} \frac{\epsilon_1}{\omega_1} [\cos(\omega_1 \zeta) - \cos(\omega_1 \tau)]. \quad (\text{B17})$$

To compare Eq. (B17) to Eq. (B16) set  $R_{\text{sc}} = 1$ , then  $\hat{R}_{\text{sc}} = \omega_p^2$  and we use the trigonometric identities

$$\begin{aligned} \cos(\alpha + \beta) + \cos(\alpha - \beta) &= 2 \cos(\alpha) \cos(\beta), \\ \cos(\alpha + \beta) - \cos(\alpha - \beta) &= -2 \sin(\alpha) \sin(\beta), \end{aligned}$$

to write Eq. (B17) as

$$z(\tau, \zeta) = \frac{1}{2} \frac{\omega_1 \epsilon_1}{\omega_p(\omega_1^2 - \omega_p^2)} \left[ \omega_1 \sin(\omega_p(\tau - \zeta)) \sin(\omega_1 \zeta) - \omega_p \cos(\omega_p(\tau - \zeta)) \cos(\omega_1 \zeta) + \omega_p \cos(\omega_1 \tau) \right] + \tau - \zeta + \frac{\epsilon_1}{2\omega_1} (\cos(\omega_1 \zeta) - \cos(\omega_1 \tau)). \quad (\text{B18})$$

For  $\omega_p \ll \omega_1$  Eq. (B18) can be reduced to Eq. (B16). For the parameters considered in this paper the results of the two expressions are graphically indistinguishable. Equations (B17), (B16), and the analogous result of Ref. [12], do not apply beyond wave breaking since the absolute value was removed from the Jacobian (B3) in their derivation.

- 
- [1] G. B. Whitham, F. R. S., *Linear and Nonlinear Waves* (Wiley, New York, 1974).
- [2] Y. Brenier, and L. Corrias, *Ann. Inst. Henri Poincaré* **15(2)**, 169 (1998).
- [3] B. Engquist, and O. Runborg, *J. Comp. Appl. Math.* **74**, 175 (1996).
- [4] B. Engquist, O. Runborg, and A.-K. Tornberg, *J. Comput. Phys.* **178**, 373 (2002).
- [5] L. Gosse, *J. Comp. Phys.* **180(1)**, 155 (2002).
- [6] S. Osher, L. T. Cheng, M. Kang, H. Shim, and Y.H. Tsai, *J. Comp. Phys.* **179(2)**, 622 (2002).
- [7] L. Gosse, S. Jin, and X.T. Li, *Math. Models Methods Appl. Sci.*, to appear.
- [8] S. Jin and X.T. Li, *Physica D* **182**, 46 (2003),
- [9] S. Jin and S. Osher, *Comm. Math. Sci.*, submitted
- [10] L.T. Cheng, H.L. Liu and S. Osher, *Comm. Math. Sci.*, submitted
- [11] S. Engelberg, H. Liu, and E. Tadmor, *Indiana University Math Journal* **50**, 109 (2001).
- [12] Y. Y. Lau, D. P. Chernin, C. Wilsen, and R. M. Gilgenbach, *IEEE Trans. Plasma Sci.* **28**, 959 (2000).
- [13] V. L. Granatstein, R. K. Parker, and C. M. Armstrong, *Proc. IEEE* **87**, 702 (1999).
- [14] R. G. E. Hutter, *Beam and Wave Electronics in Microwave Tubes* (D. Van Nostrand Company, Inc., Princeton, 1960).
- [15] C. Sparber, P. Markowich, and N.J. Mauser, *Nonlinear Analysis* **33**, 153 (2003),
- [16] C. Cercignani, *The Boltzmann Equation and its Applications*, vol. 67 of *Applied Mathematical Sciences* (Springer-Verlag, New York, 1988).
- [17] H. Grad, *Phys. Fluids* **6**, 147 (1963).
- [18] C. D. Levermore, *J. Stat. Phys* **83**, 1021 (1996).
- [19] C. B. Wilsen, Ph.D. thesis, University of Michigan, Ann Arbor (2001).
- [20] S. Bhattacharjee, C. Marchewka, J. Welter, R. Kowalczyk, C. Wilsen, Y. Lau, J. Booske, A. Singh, J. Scharer, R. Gilgenbach, et al., *Phys. Rev. Lett.* **90** (2003), article 098303.
- [21] C. Wilsen, Y. Y. Lau, D. P. Chernin, and R. M. Gilgenbach, *IEEE Trans. Plasma Sci.* **30**, 1176 (2002).
- [22]  $R_{sc}$  as it appears in (1) is related to the space charge reduction factor  $R$  of Ref. [14] by  $R_{sc} = R^2$ .
- [23] In practice  $N_{max}$  is only limited by the availability of an expression for  $\phi_{N_{max}-1}$ .
- [24] To arrive at this result one combines the first of Eqs. (A1), Eq. (5), and Eq. (C1) of Ref. [12].